New Techniques Enable Comparative Analysis of Microtubule Orientation, Wall Texture, and Growth Rate in Intact Roots of Arabidopsis

Keiko Sugimoto[1], Richard E. Williamson, and Geoffrey O. Wasteneys*

Plant Cell Biology Group, Research School of Biological Sciences, Australian National University, Canberra, Australian Capital Territory 2601, Australia

This article explores root epidermal cell elongation and its dependence on two structural elements of cells, cortical microtubules and cellulose microfibrils. The recent identification of Arabidopsis morphology mutants with putative cell wall or cytoskeletal defects demands a procedure for examining and comparing wall architecture and microtubule organization patterns in this species. We developed methods to examine cellulose microfibrils by field emission scanning electron microscopy and microtubules by immunofluorescence in essentially intact roots. We were able to compare cellulose microfibril and microtubule alignment patterns at equivalent stages of cell expansion. Field emission scanning electron microscopy revealed that Arabidopsis root epidermal cells have typical dicot primary cell wall structure with prominent transverse cellulose microfibrils embedded in pectic substances. Our analysis showed that microtubules and microfibrils have similar orientation only during the initial phase of elongation growth. Microtubule patterns deviate from a predominantly transverse orientation while cells are still expanding, whereas cellulose microfibrils remain transverse until well after expansion finishes. We also observed microtubule-microfibril alignment discord before cells enter their elongation phase. This study and the new technology it presents provide a starting point for further investigations on the physical properties of cell walls and their mechanisms of assembly.

Cell elongation and the direction of organ expansion are linked processes of functional importance in plant development. The structural features of the plant cell wall along with its physiological activity dictate the mechanical properties that regulate the rate and direction of cell expansion. The arrangement of newly synthesized cellulose microfibrils (CMFs) is thought to play a prominent role in determining these properties (Preston, 1974; Taiz, 1984; Carpita and Gibeaut, 1993) and cortical microtubules (CMTs) are usually implicated in the alignment of CMFs. Two broad questions remain to be answered: (a) How does wall structure relate to the rate and/or direction of expansion? (b) What role do CMTs play in determining wall structure, growth rates, and other features of cell expansion?

The most favored but as yet unproven model for CMF alignment in diffusely expanding cells suggests that movement of cellulose synthase complexes (rosettes) along plasma membranes is driven by cellulose crystallization but guided by CMTs (Herth, 1980; Giddings and Staehelin, 1991). CMTs fit quite nicely as the likely modulator of cellulose alignment but many lingering doubts remain. Previous descriptions by transmission electron microscopy of CMTs in similar orientations to CMFs are limited to very tiny areas of cells (Palevitz and Hepler, 1976; Hardham et al., 1980; Seagull and Heath, 1980; Vesk et al., 1996). Furthermore, the striations seen in glutaraldehyde-fixed, uranyl acetate/lead citrate stained thin sections have been shown to not be CMFs in *Equisetum hyemale* root hairs (Emons, 1988), raising some doubt as to their assumed identity in earlier studies (Palevitz and Hepler, 1976; Hardham et al., 1980; Seagull and Heath, 1980). Fluorescent probes that localize CMFs have been used for observing CMF-CMT co-alignment during xylogenesis (Falconer and Seagull, 1986), protoplast regeneration (Galway and Hardham, 1989; Hasezawa and Nozaki, 1999), and cotton fiber development (Seagull, 1986). The method, however, has low resolution and lacks clarity when applied to analyze primary walls in multicellular tissues (Sauter et al., 1993).

An indirect but more compelling proof of CMT function is that CMT disruption leads to isotropic cell expansion (Green, 1962) or that it prevents the establishment of a dominant axis of polarity (Galway and Hardham, 1986). Some studies have demonstrated that CMT destabilizing drugs cause disordered CMFs (Green, 1962; Hogetsu and Shibaoka, 1978; Marchant and Hines, 1979; Robinson and Quader, 1982; Richmond, 1983) but in most cases the alignment of CMFs has been determined by birefringence patterns and not confirmed at the ultrastructural level. Other observations of inconsistent or nonexistent CMT-CMF co-alignment have led to questioning of the role

[1] Present address: Department of Cell Biology, John Innes Centre, Colney, Norwich, NR4 7UH, UK.

* Corresponding author; e-mail geoffw@rsbs.anu.edu.au; fax 61–0–2–6125–4331.

CMTs play in aligning CMFs (Itoh, 1976; Srivastava et al., 1976; Preston, 1988; Kimura and Mizuta, 1994).

The plethora of Arabidopsis root mutants (Baskin et al., 1992a; Benfey and Schiefelbein, 1994; Hauser et al., 1995) is helping to identify key root morphology genes (Arioli et al., 1998), many of which have broader roles in plant development. Understanding the role of wall structure in cell growth and morphogenesis is an essential adjunct to the molecular-genetic studies. Fortunately, Arabidopsis roots are also ideal experimental systems with a predictable and simple anatomy (Dolan et al., 1993) that remains uniform throughout root growth (Esau, 1977). They are highly anisotropic; once cells leave the cell division zone, there is no appreciable radial expansion (Baskin et al., 1992a), and individual cell growth is completed in a matter of hours. In this article we present methods for examining CMF and CMT patterns in Arabidopsis root epidermal cells. We then describe and compare CMT and CMF alignment patterns in relation to growth kinetics of the wild-type root under standard culture conditions.

RESULTS

Our goal was to describe and compare CMF and CMT patterns in relation to the growth and development of epidermal cells in the wild-type Arabidopsis root. To achieve this, we required methods enabling analysis of wall texture and CMT patterns in root tips that remained essentially intact so that the stage of development of each cell could be unequivocally determined. In addition, we wanted methods that were sufficiently reliable and simple to allow their routine application in experimental studies and in mutant characterization.

Root Growth and Elongation Profile

The consistent nature of Arabidopsis root growth on vertical agar plates was critical to the correlative nature of this study. Under standardized culture conditions, root elongation rates increased gradually with time, from 0.15 ± 0.02 mm h^{-1} at d 4 to 0.24 ± 0.04 mm h^{-1} at d 8, while root diameter remained relatively constant at 0.14 ± 0.004 mm. Baskin et al. (1992a) reported identical results. For all experiments, plants were analyzed precisely 5 d after planting to avoid age-dependent differences in growth profiles. Spatial distribution of root growth along this axis was determined by marking the surface of roots with carbon grains and then measuring the separation of two consecutive grains after a set time interval (Fig. 1, A and B). Figure 1C depicts relative elemental growth rate (REGR) at set points along the root axis. Roots exhibited a characteristic bell-shaped axial growth curve with growth accelerating in the region 0.25 to 0.375 mm from the root apex, peaking around 0.625 mm, and then declining until it was undetectable around the 1.25-mm point. This growth profile accords with the recent measurements of Mullen et al. (1998), who used a similar marker movement method, and Baskin et al. (1995), who deduced REGRs from kinematic measurements.

Field Emission Scanning Electron Microscopy (FESEM) Examination of CMF Patterns throughout Root Development

To accurately analyze CMF patterns at precise stages of cell growth, we needed to first develop a method for examining cell walls in roots that retained continuous files of epidermal cells. The best way to

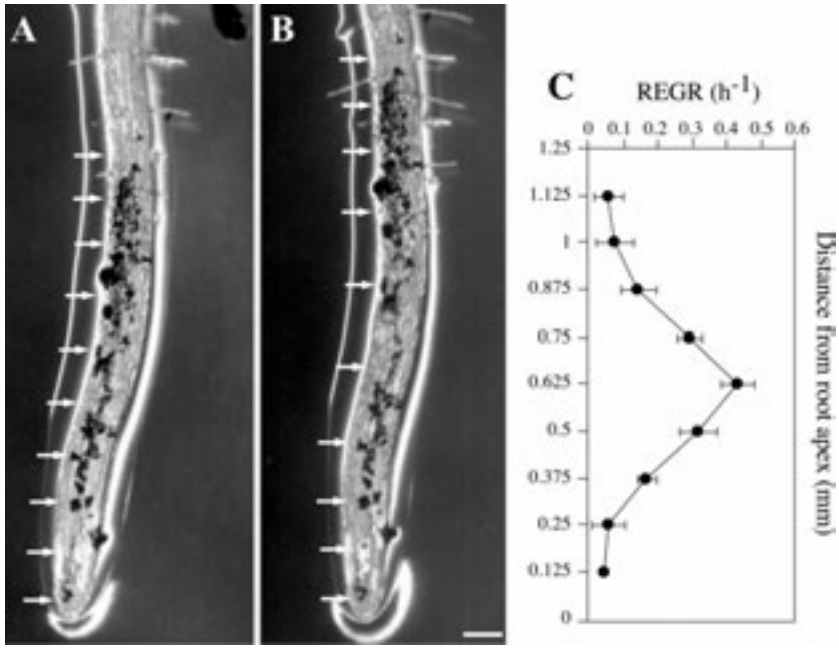

Figure 1. Spatial distribution of root elongation 5 d after germination under standard growth conditions. A, Root tip labeled with carbon grains showing positions of carbon grains at set increments. B, One hour later, the separation of carbon grains identifies the elongation zone. Bar = 100 μm. C, The growth profile of 5-d root tips (n = 30), calculated by measuring carbon grain separation, indicates that growth accelerates between 0.25 and 0.375 mm from the tip, reaches a maximum at approximately 0.625 mm, and declines to zero at 1.25 mm.

achieve this was to remove one or more longitudinal cryosections to expose an internal surface in the fixed root and then extract sufficient cytoplasm to reveal wall texture in the exposed cells without compromising the root tip's integrity (Fig. 2). In favorably oriented roots this enabled analysis of wall structures in cells at every stage of cellular development from the root cap to beyond the elongation zone. Epidermal cells were identified most reliably along the edge of the cut (those in the center were often cortex or endodermal cells) so most images were collected from the radial rather than inner tangential wall surfaces. As shown in Figure 3A, the cell walls were occluded by cytoplasm if no extraction were attempted. Several extraction procedures were compared. Chloroform/methanol, used to solubilize lipids from crude cell wall fractions, removed relatively little material and only occasionally revealed underlying cell wall structures (Fig. 3B). Two detergents, saponin and Triton X-100 at 1% (v/v), both removed substantial material and revealed wall structures in some places but only after vigorous shaking for 48 h at 30°C (Fig. 3, C and D, respectively). By comparison, 10-min treatment with 0.1% (v/v) sodium hypochlorite removed cytoplasmic material effectively and clearly (Fig. 4). This gave the most reliable results without altering the integrity of the specimen and was used for all subsequent analysis of wall structure.

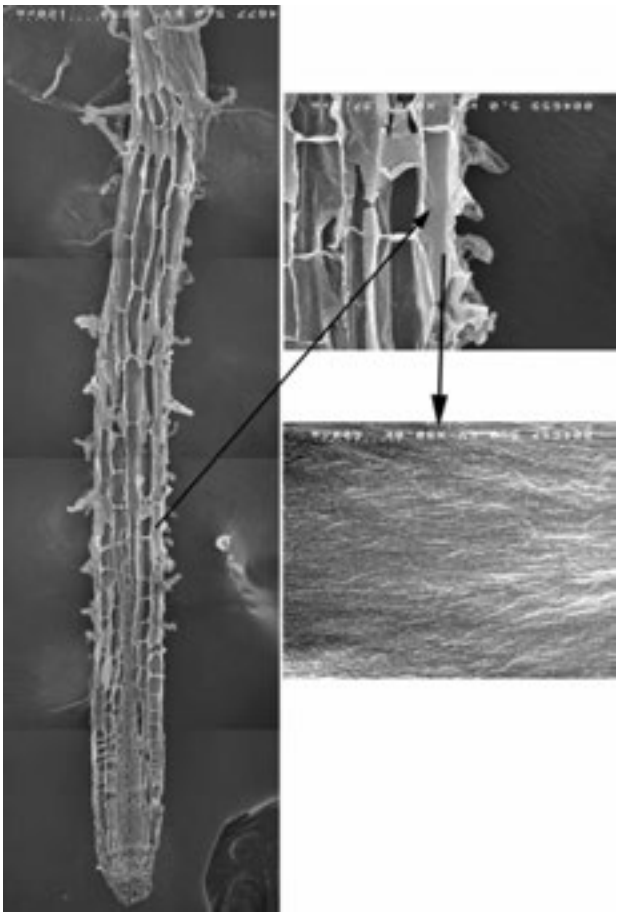

Figure 2. Procedure for FESEM observation of walls from Arabidopsis root tips. Longitudinal cryosectioning removes the outer layer of the root so that after extraction, critical-point drying, and coating with platinum, the microfibrillar texture of nearly every cell can be examined.

Characteristics of Primary Walls of Root Epidermal Cells

As shown in Figure 4A, the innermost layer of the root epidermal cell wall was mainly composed of transversely aligned fibrous structures. The fibers had fairly uniform diameter, between 10 and 20 nm (including the 2.5-nm thickness of platinum coating) but thin fibers around 5 nm or thicker bundles around 30 nm in diameter were observed occasionally. Other very short fibrous structures around 60 nm in length and 5 nm in diameter were also abundant (Fig. 4A, arrowheads). These shorter fibers lay at right angles across a few of the longer transverse fibers. Both fibrous structures were generally embedded in amorphous material that was absent after extensive acid extraction (Fig. 5A). Pit fields, from which all fibrous structures were excluded, were also common (Fig. 4A, asterisk). In contrast, examining the external face of the outer tangential wall of the root epidermal cells revealed several layers of loosely and randomly aligned fibers 30 to 40 nm in diameter (Fig. 4B). Compared with the internal face, short fibrous components were not detected and, as judged by the clarity of the fibrous structures, matrix material was less abundant.

Cellulosic Identity of Microfibrillar Structures

Several extraction analyses with acids, polysaccharide-degrading enzymes, and proteases confirmed that the dominant fibrous structures depicted in samples extracted with sodium hypochlorite were CMFs. Boiling seedlings in an acetic acid-nitric acid mixture extracts everything except crystalline cellulose (McCann et al., 1990). On our cryo-sectioned samples, this thorough extraction procedure revealed a very well-defined wall texture (Fig. 5A), although the fibrous structures were somewhat rearranged and aggregated. Figure 5B shows how a relatively mild, 1-h digestion with 0.1% (w/v) Cellulysin, which degrades crystalline cellulose, reduced the proportion of fibrous material. Longer treatments rendered samples useless for examination. Pectolyase, which contains mainly endo-polygalacturonase and endo-pectin lyase, removed non-fibrous material and created numerous large pores when applied at 0.1% (Fig. 5C) but left the long transverse fibrous structures essentially intact. Neither endo-1,4-β-glucanase (Fig. 5D), which degrades xyloglucan and non-crystalline cellulose but not crystalline cellulose, nor protease (Fig. 5E) caused any change to the over-

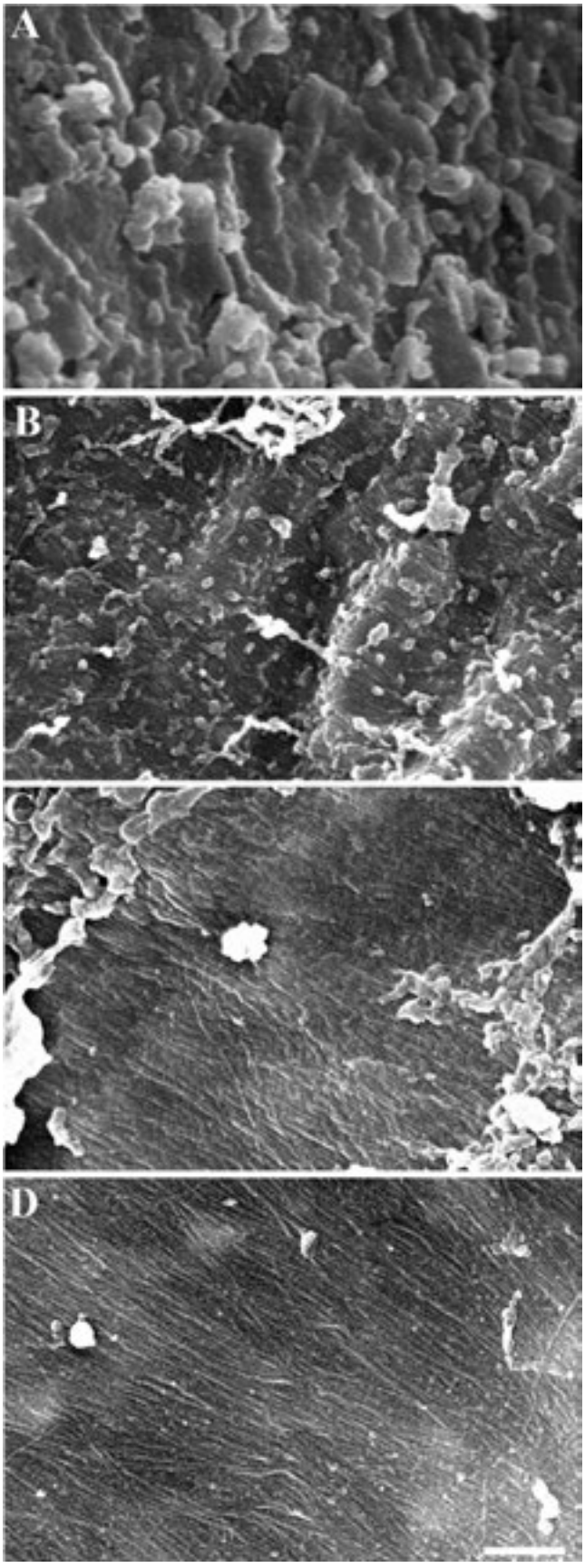

all wall structure or removed any specific components. This diagnosis is consistent with observations reported for other species (McCann et al., 1990; Carpita and Gibeaut, 1993), depicting transverse CMFs embedded in pectic polysaccharides.

CMFs Remain Transverse throughout Elongation

Figure 6 shows a low magnification micrograph of one example of a root from which cryosections have been removed, along with high magnification images depicting CMF patterns from specific cells, as indicated, along this root's length (Fig. 6, A–F). CMFs were predominantly transversely aligned throughout the cell division zone (Fig. 6A). The presence of pit fields, which occupy relatively large proportions of the smaller cells of the division zone, caused localized deviation of CMFs. Apart from this, CMFs deviated very little from the transverse axis, as revealed by quantitative analysis (Fig. 7C). CMFs remained transverse throughout (Fig. 6, B–D) and even beyond the elongation zone (Fig. 6E). The only detectable difference during this period was that CMFs in younger cells, i.e. those in mitotic and early elongation zones (Fig. 6, A–C), were less distinct than those in older, non-expanding cells (Fig. 6, D and E), perhaps because of changes in matrix quantity in their walls. The occurrence of non-transverse, short fibers varied from sample to sample but there was no clear trend with respect to their abundance in relation to the stage of cell expansion.

Groups of obliquely aligned CMFs were detected 1.9 mm or further from the root apex, where cell expansion was complete (Fig. 6F). These oblique CMFs generally ran in groups of 10 to 20 roughly parallel fibrils. In addition, their alignment seemed to shift abruptly from transverse to nearly 45 degrees to the long axis without any obvious transition region. Quantitative analysis of CMF angular dispersion revealed that they only deviated significantly from transverse alignment in the region further than 1.5 mm from the root apex (Fig. 7C). CMF deviation from the transverse axis conformed to a right handed or Z-form helix as conventionally determined by viewing from outside the cell.

Whole Mount Immunofluorescence and Confocal Microscopy

CMT patterns were recorded from immunolabeled intact root tips using confocal laser scanning micros-

Figure 3. Comparison of extraction methods for preparing root tissues for FESEM analysis following fixation and cryosectioning away the outer layer. After extraction, all specimens were osmicated, dehydrated, critical point dried, and platinum-coated. A, With no treatment, cytoplasmic debris occludes cell wall. B, Chloroform-methanol (1:1) treatment for 1 h at 40°C removes only some cytoplasmic material. C, One percent (v/v) saponin for 48 h at 30°C reveals patches of wall material. D, One percent (v/v) Triton X-100 for 48 h at 30°C is quite effective but takes considerable time. Bar = 300 nm.

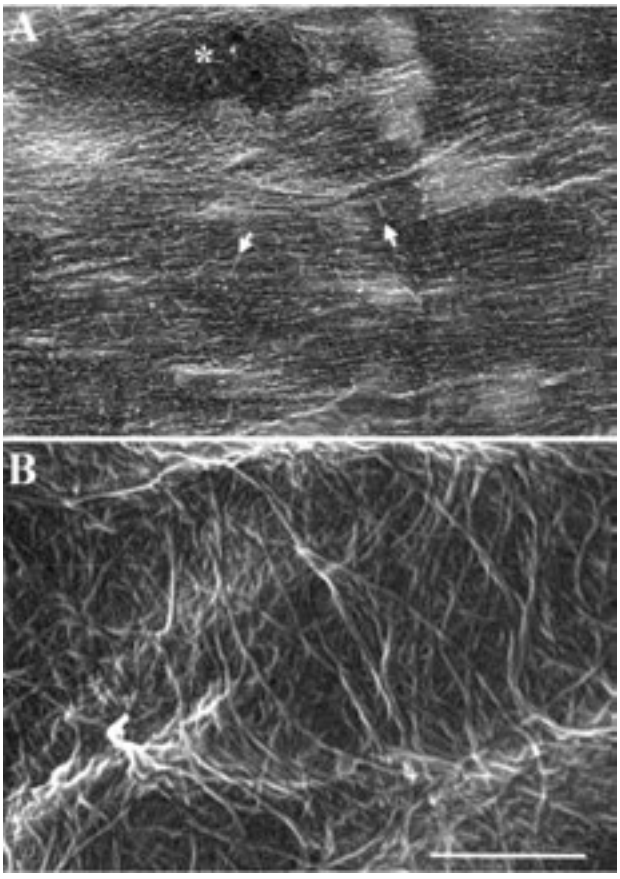

Figure 4. Wall texture differs on inner (A) and outer (B) face of a root epidermal cell. FESEM specimens were prepared by extracting with 0.1% (v/v) sodium hypochlorite for 10 min, a method that is fast and causes moderate but consistent extraction. Images are oriented so that the transverse cell axis is parallel to the short axis of the page. A, The most recently deposited layer, i.e. the layer closest to the plasma membrane, has prominent transverse fibrils across which lie short fibers (arrows). Pit fields (asterisk) were frequently seen. B, The texture differed considerably on the outer face of epidermal cells. Microfibrils have no preferred orientation and vary greatly in apparent thickness. The more open texture and ability to distinguish several lamina suggest matrix material is less abundant than at the inner wall surface. Bar = 600 nm.

copy. The method included a mild enzymatic digestion (see Fig. 5C for pectolyase treatment) and cold methanol treatment, and labeled CMTs in nearly all epidermal root tip cells, except those beyond the elongation zone, which were permeabilized unreliably. This enabled CMT orientation patterns to be analyzed in cells at known REGRs.

Changes in CMT Orientation Preceded Growth Cessation and Changes in CMF Patterns

Figure 8A shows a typical image of anti-tubulin labeling of CMTs in root epidermal cells at d 5. CMTs were detected in cells from the root cap and in epidermal cells in the late cell division and elongation zones, which emerge from beneath the root cap. In the root cap cells, CMTs were predominantly transverse in orientation. In the distal cell division zone, where growth rates were still low, CMTs deviated considerably about the transverse axis (Fig. 8B; see also large SD of CMT alignment at 0.2 mm in Fig. 7B). Once the longitudinal axis of the cell exceeded the radial axis, however, CMTs were consistently transversely aligned in parallel arrays, and such alignment was maintained while growth rates were increasing (Figs. 7, A and B and 8, C–E). In the region where growth was starting to decline, CMTs were far less numerous and, in some cells, were obliquely oriented (Fig. 8F). CMTs in these cells formed shallow helices that were consistently right-handed (of Z-helix form, when viewed from outside the cell). Nearing completion of elongation, CMTs varied from transverse through oblique to longitudinal within individual cells (Fig. 8G). There was no obvious difference between CMT patterns in trichoblasts versus atrichoblasts. (Trichoblasts could be identified by the emergence of root hairs at the apical end of cells in the same files.) Adjacent cells, however, frequently showed considerable variation in CMT orientation patterns despite having the same REGR (compare CMT patterns in adjacent cells in Fig. 8G).

One potential drawback of our method was that CMF images were collected from the radial or, less often, the inner tangential wall surfaces, whereas the confocal scans of CMTs were mainly projected from the perspective of the outer tangential wall. Lack of CMT-CMF congruence during the phase of declining REGR could conceivably be attributed to CMTs changing orientation on the outer tangential surface but remaining transverse along the radial and inner tangential walls. We disproved this possibility. Figure 8F is projected so that optical sections from the entire cells are displayed. The criss-crossing of CMTs indicates that the inner tangential wall CMTs continue the right-handed spiral configuration and U-shaped bends show that CMTs also deviate from the transverse axis to the same extent on all longitudinal surfaces. We also performed digital rotations of Z-series projections. As demonstrated in Figure 8, H–J, CMTs are obliquely oriented on the radial cell surfaces with the same handedness as on the outer tangential surface.

These results clearly indicate that CMTs are predominantly transverse during the early phase of elongation but gradually shift to oblique and then longitudinal orientations as REGR declines. Quantitative analysis of CMT alignment along the major root axis revealed that the shift from transverse to oblique orientation starts around 0.7 mm from the root apex and gradually proceeds until CMTs are predominantly longitudinally aligned at around 0.9 mm (Fig. 7B).

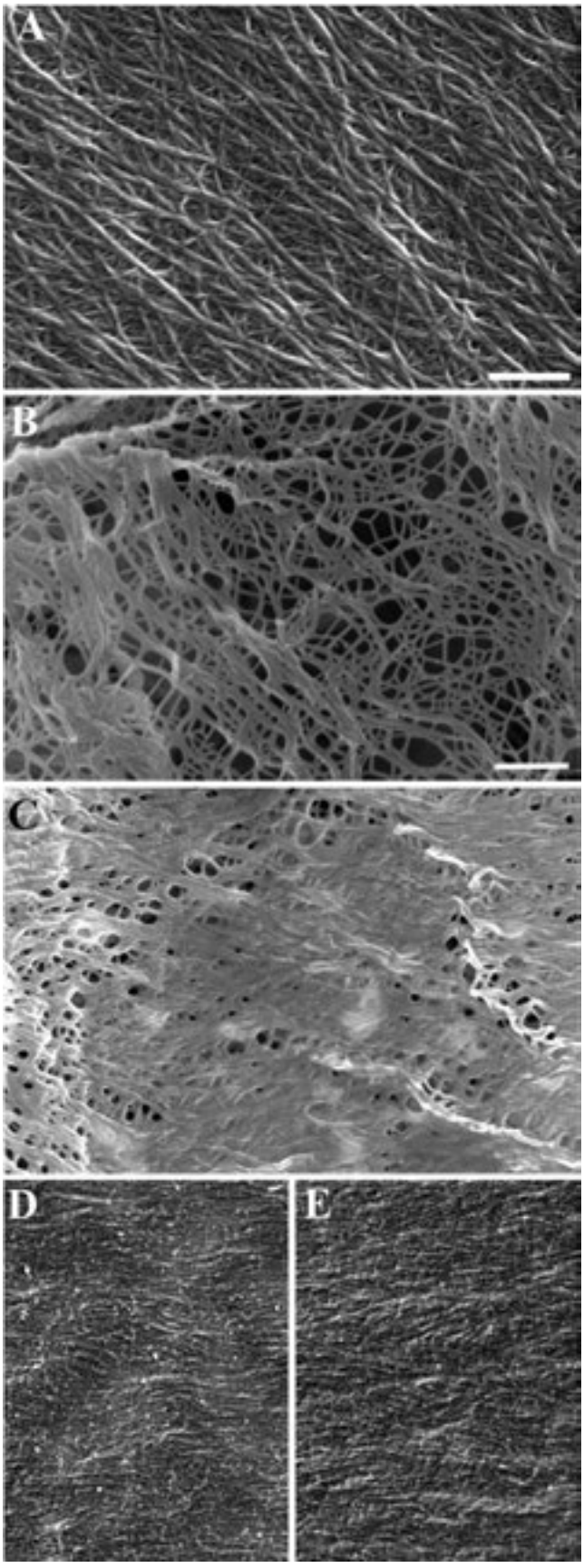

DISCUSSION

This study provides a detailed comparison of CMT and CMF orientation patterns in epidermal cells throughout cell growth. Elongation rates (REGR) were measured directly from living roots the same age as and grown under identical conditions to the specimens sampled for wall or CMT analysis. By keeping root tips intact while preparing specimens for immunolabeling or FESEM analysis, we could identify the growth status of any cell with reasonable accuracy. We found that CMT and CMF orientation patterns were similar only during the period of accelerating elongation. CMFs were transverse to the root's long axis from the cell division zone through to and beyond the elongation zone. CMT orientation, however, was variable in the cell division zone, transverse in the first half of the elongation zone, and began to deviate from the transverse axis once REGR began to decline. Despite this change in CMT orientation during the later stages of growth, cell expansion remained anisotropic, with no appreciable increase in root diameter throughout or beyond the elongation zone. CMTs consistently formed right-handed helices as they deviated from the transverse axis. Well after cell expansion stopped, CMFs were observed sporadically in oblique orientations that also deviated in a right-handed manner though by this stage, most CMTs were oriented nearly longitudinally. The ensuing discussion addresses the technical aspects of this work along with the implications of our findings for current theory on plant cell wall construction.

FESEM Observations of the Walls of in Situ Cells

High resolution methods for accurately imaging recently deposited CMFs are critical for elucidating the role these elements play in cell expansion. Ultrathin sections examined by transmission electron microscopy can reveal striations in the wall, assumed to be CMFs (Preston, 1974; Sawhney and Srivastava, 1975; Hardham et al., 1980; Lang et al., 1982) but, as Emons (1988) has demonstrated, these striations do not always represent CMFs. Freeze-etching (Preston, 1974; Mueller and Brown, 1980), dry-cleaving (Sassen et al., 1985; Emons, 1988), deep etching (McCann et al., 1990), and replica methods (Green, 1958) are more

Figure 5. Comparative chemical and enzymatic treatments helped identify the chemical nature of cell wall components. A, Boiling in acetic acid:nitric acid:distilled water (8:1:2) for 1 h thoroughly extracted the cytoplasm and wall matrix but CMFs are retained. B, Cellulysin (0.1%, w/v) severely degraded and ruptured the wall, leaving an open meshwork of residual material, consistent with the predominant fibrous material being cellulose. C, Pectolyase (0.1%, w/v) removed non-fibrous material, modified the arrangement of fibrils, and created numerous holes in the wall. In contrast, treatment with 0.125 units mL^{-1} endo-1,4-β-glucanase (D) or protease (E) had no detectable effect on wall texture. Bars (bar in B is for B–E) = 300 nm.

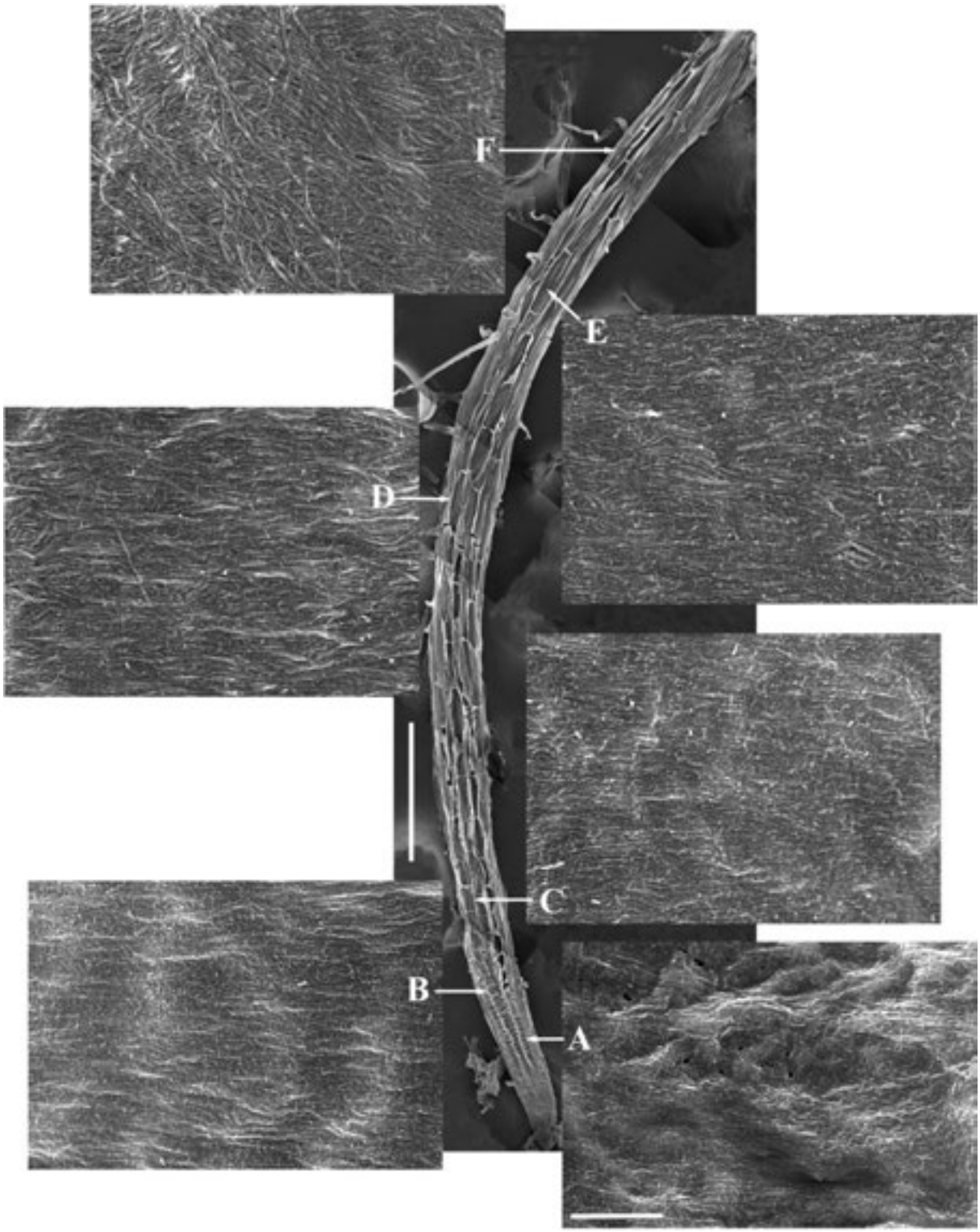

Figure 6. Developmental progression of wall texture in root tip from cell division zone to differentiation zone. The low-magnification image of the root indicates the extracted cells from which the higher magnification FESEM images (A–F) were taken. Micrographs are oriented to show microfibril alignment relative to the cell and root long axis, not the orientation of the root, which warped slightly during processing. In the cell division zone (A) microfibril alignment is already predominantly transverse. Note numerous pit fields, undulating texture, and predominantly transverse microfibril alignment. Microfibril orientation remains predominantly transverse throughout the elongation zone (B and C), at the time of (D) and after growth cessation (E). F, Deviation of CMFs from the transverse axis was first detected approximately 2 mm from the tip where root hairs are well developed. Bar for whole root image = 250 μm. Bar for A through E = 500 nm.

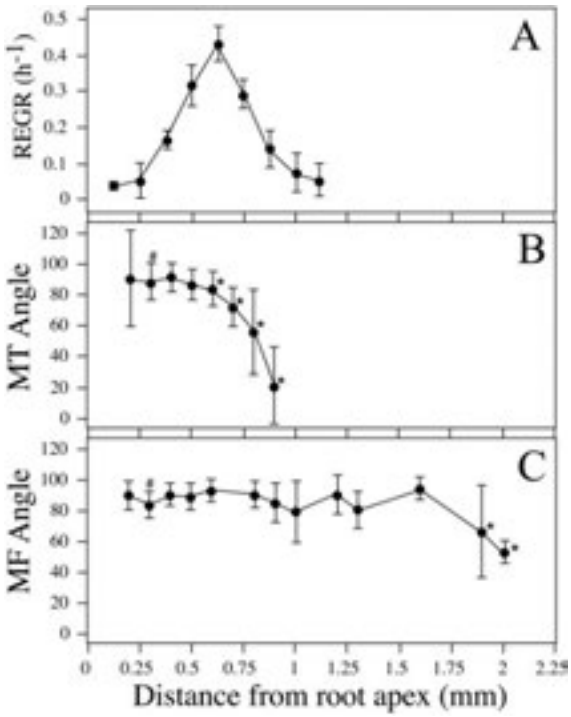

Figure 7. CMT and CMF orientation relative to the cell long axis plotted against distance from root apex in d 5 root tips. REGR, replotted from Figure 4C. Mean microtubule angle (degrees) deviates from the transverse axis about the time REGR begins to decline (B). In contrast, CMFs remain predominantly transverse until well after growth has ceased (C). Values are means from six roots (microtubules), three roots (microfibrils), and 30 roots (REGR) with SD indicated by error bars. All data points differing significantly from the measured mean orientation at 0.3 mm from the root apex (#), as determined by the independent Student's *t* test, are indicated as (*).

suitable but limited. Generally only small portions of cell walls are visible and the lack of control over where observations can be made make it difficult to correlate wall texture to growth kinetics and/or CMT patterns. Our protocol, involving cryo-sectioning the root tip followed by cytoplasmic extraction and shadow-casting, overcomes these problems. It was possible to view the innermost layer of cell walls at any position along roots while maintaining the intact root structure so that CMF orientation could be measured with respect to the axis of expansion.

Field emission electron sources produce scanning electron micrographic images at outstandingly high spatial resolution by providing small diameter beams of high brightness (Crewe et al., 1968) and low accelerating voltages (Pawley and Erlandsen, 1989). In plants, FESEMs use so far has been limited to simultaneously viewing CMTs and cell walls in partially extracted onion root tips (Vesk et al., 1994) and tobacco BY-2 cells (Vesk et al., 1996) and determining the alignment of CMFs in some woody species (Abe et al., 1995; Prodhan et al., 1995). To view the innermost layer of primary cell walls, we planed a thin layer from the frozen root surface and gently ex-

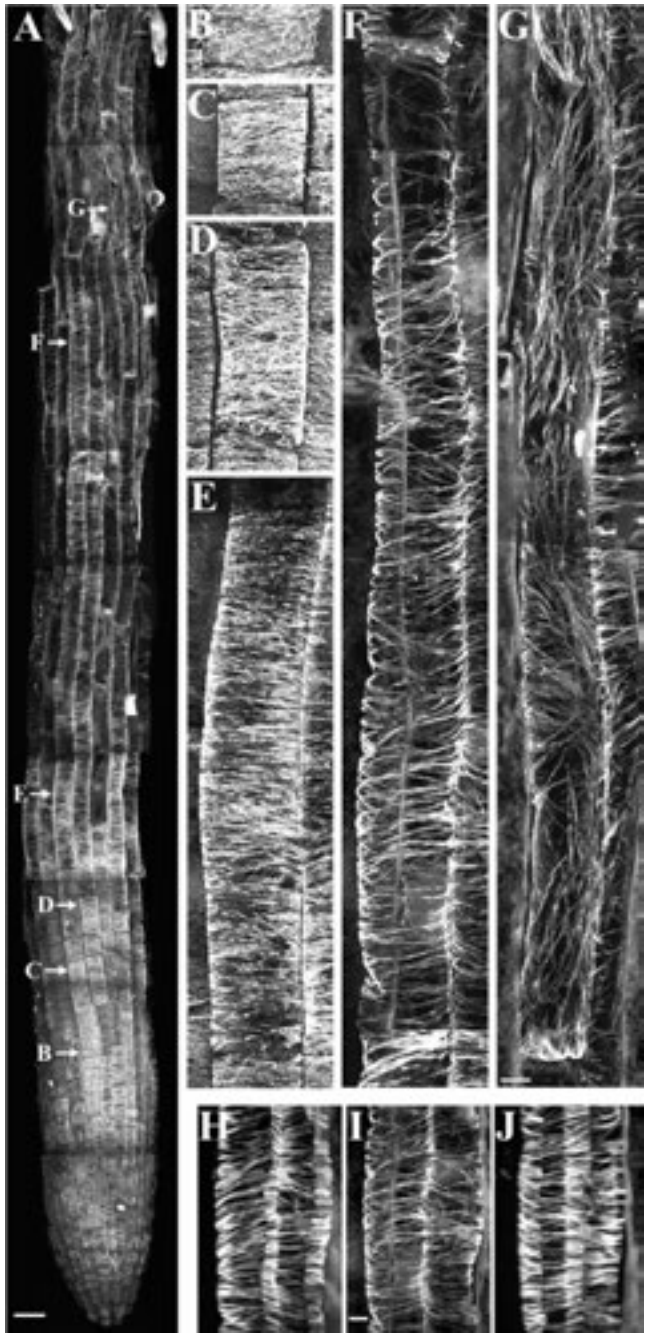

Figure 8. Confocal micrographs of immunolabelled microtubules in an intact root tip (A) and at higher magnification in selected cells from the same root tip (B–G). Root cap cells obscure epidermal cells in much of the cell division zone (A). CMTs were variably oriented in the cell division zone (B), predominantly transverse during the phase of increasing REGR (C–E), and oblique to longitudinal as REGRs declined (F and G). Rotation of a confocal optical series projection from region F reveals that oblique microtubule orientation is consistent around the circumference of the cell (H–J). The original projection (I) is rotated 40° to the left (H) and right (J) to indicate microtubule alignment on the radial wall surfaces. Bar in A = 25 μm. Bar for B through G in G = 5 μm. Bar for H through J = 5 μm.

tracted cytoplasmic material from the exposed cells with sodium hypochlorite. Conventional sliding microtomes are often used for cryo-sectioning (Takeda and Shibaoka, 1978; Hogetsu, 1986; Abe et al., 1995; Prodhan et al., 1995) but in this study, a cryo-ultramicrotome cooled to −120°C with liquid N_2 was used to prevent structural deformation by ice crystals. Dimethyl sulfoxide (DMSO) was used as a cryoprotectant for the same reason. The innermost layer of cell wall was covered with cytoplasm, in contrast to reports for other species using replica techniques (Takeda and Shibaoka, 1978; Hogetsu, 1986), and treatment with sodium hypochlorite was found to be most effective for removing this material. What hypochlorite extracts from cells is not fully understood, although it has been used to extract cytoplasm from woody tissue (Abe et al., 1995). From its chemical structure it is likely that hypochlorite only interacts with proteins and not polysaccharides. Furthermore, the wall structure observed with this rapid extraction procedure was similar to that obtained after extraction by milder but longer detergent treatments. From these observations it is very likely we were able to observe a good representation of nascent cell wall structure.

Primary Cell Walls of Arabidopsis Root Cells

FESEM revealed several fine structural details of Arabidopsis primary cell walls. The transverse fibrous structures are most likely to be CMFs based on the following evidence. (a) The diameter of these fibrils was 10 to 20 nm. Taking approximately 2.5-nm thickness of platinum coating into account, this is in good agreement with the reported diameter of cellulose, 5 to 12 nm, in higher plants (Brown, 1982; McCann et al., 1990). (b) They were only digested by Cellulysin but not by other tested enzymes. (c) They were aligned predominantly transversely in expanding root cells as previously noted in many studies (e.g. Gunning and Hardham, 1982). (d) Although modified, they survived boiling in nitric-acetic acid, a treatment that crystalline cellulose but not other polysaccharides can withstand (McCann et al., 1990). There were additional short but still fibrous structures observed in the primary walls. These were approximately 60 nm in length, approximately 5 nm in diameter, and ran at right angles across a few adjacent CMFs. These fibers were most likely hemicellulosic even though endo-1,4-β-glucanase did not appear to remove them. Similar structures were observed in onion cells (McCann et al., 1990) and were suggested to be hemicellulosic based on the fact that they were extractable with alkali. The nonfibrous structures observed on these walls were probably pectins as they were only extractable with pectolyase. In general, our observations demonstrated that Arabidopsis root epidermal cells have typical dicot primary cell wall architecture (McCann and Roberts, 1991; Carpita and Gibeaut, 1993). Further confirmation of the chemical nature of each structure will be achieved in future work by labeling cellulose with gold-conjugated cellulases, immunolabelling pectins (Knox, 1992; Willats and Knox, 1999), and chemical extraction of hemicelluloses.

CMF Alignment Corresponds to Growth Anisotropy But Not Growth Rate

FESEM revealed that CMFs remained predominantly transverse well after growth rates started to decline and that they only became sporadically oblique long after cells ceased elongating. These observations support the view that CMF alignment regulates the direction but not the rate of cell expansion (Baskin et al., 1999). Instead, factors that control the rigidification of cell walls regulate the decline and cessation of cell elongation (Pritchard et al., 1993; Cosgrove, 1997), whereas turgor remains more or less constant (Pritchard et al., 1993). These factors probably act in processes such as reducing wall loosening, increasing wall cross-linking activities, and/or altering the composition of the other wall polysaccharides to make the wall more rigid or less susceptible to wall loosening.

Assessment of Immunofluorescence Protocol

To study developmental changes in CMT organization patterns, it is essential to label the full range of cells within a developing tissue. This has been achieved with epidermal peels (Roberts et al., 1985), internodal strips (Flanders et al., 1990), partially digested shoot apical meristems (Marc and Hackett, 1989), and wax or plastic resin sections of roots (Baluska et al., 1992; Baskin et al., 1992b; Liang et al., 1996). We combined mild enzymatic digestion of cell walls with cold methanol treatment to obtain consistent CMT labeling in nearly all epidermal root tip cells. Unlike the laborious processes of embedding and sectioning, this protocol allows us to process large numbers of samples. Furthermore, since the whole structure of each cell is very well preserved, one can reconstruct accurate three-dimensional patterns from confocal Z-series. This method is also quite useful to study the effects of drugs and/or mutations on the arrangement of CMTs in cells at various developmental stages and could probably be adapted for wide ranging applications including in situ hybridization, for the analysis of gene expression patterns.

Establishing Transverse CMT Orientation in the Early Elongation Zone

In this study, we demonstrated that CMTs in Arabidopsis root epidermal cells undergo a series of conformational changes according to the develop-

mental stages of cells. Although CMT orientation is relatively variable in the cell division zone, CMTs become consistently transverse as soon as elongation growth is detected. This is consistent with observations made in a wide range of cell types (Clayton et al., 1985; Wick, 1985; Flanders et al., 1990; Nagata and Hasezawa, 1993; Baskin et al., 1999; Bichet et al., 2000; Wenzel et al., 2000). Arabidopsis mutants with apparently normal division patterns but random cortical arrays including *fass* (McClinton and Sung, 1997) and *botero1* (Bichet et al., 2000) may help identify the mechanism for establishing transverse CMTs. In the *botero1* mutant, CMTs fail to consolidate into transverse arrays as cells enter the elongation zone and growth anisotropy is impaired (Bichet et al., 2000).

CMTs and Growth Rate Decline

This study revealed that CMTs start to become oblique as soon as elongation rates start to decline (Fig. 7, A and B). The following observations, however, strongly suggest that mechanisms controlling growth rates are independent of CMT orientation. First, CMT patterns varied considerably between adjacent cells that necessarily had identical growth rates (note the large SD for CMT alignment at 0.8 and 0.9 mm in Fig. 7B). Traas et al. (1984) and Baluska et al. (1992) also reported that oblique CMTs did not appear simultaneously in all cells, suggesting that these shifts are only incidental features accompanying the decline of elongation. The pattern of CMT deviation from the transverse axis is also clearly variable from one cell type to another. In pea (Hogetsu and Oshima, 1986) and maize (Baskin et al., 1999) roots, re-orientation of CMTs begins only well after cell elongation starts to slow down. In barley leaves, CMTs remain predominantly transverse throughout the elongation zone but in GA-deficient mutants, CMTs lose transverse order in the distal elongation zone (Wenzel et al., 2000). Wasteneys and Williamson (1987, 1993) reported that internodal cells of two characean genera show remarkable differences in the CMT transition patterns during the cessation of their growth, yet these do not result in any obvious differences in growth dynamics or morphology.

Whether the decline in the elongation rate causes shifts in CMT orientation has also been addressed. Earlier work suggested that strain might play a role in determining CMT orientation (Wasteneys and Williamson, 1987), but four studies prove otherwise. When organ growth was perturbed by experimental conditions such as irradiating pea stems with blue light (Laskowski, 1990), treating *Nitella* internodes with pH band-inducing medium (Kropf et al., 1997), and keeping auxin-treated azuki bean epicotyls in anaerobic conditions (Takesue and Shibaoka, 1999), CMTs remained or became transverse after cell elongation declined or even ceased altogether. In maize pulvinal cells, CMTs remain transverse for many days despite zero growth activity (Collings et al., 1998), suggesting that CMT orientation is not influenced by elongation rate.

Role of CMTs in Aligning CMFs

We determined that CMTs and CMFs are both transversely aligned with relatively small standard deviations in the region of the root where REGR is rising. This agrees with previous reports for roots of other taxa (Gunning and Hardham, 1982; Hogetsu, 1986; Baskin et al., 1999) but we also found that CMTs are not as uniformly transverse as CMFs in the cell division-elongation transition zone and that CMTs and CMFs have contrasting orientations in the distal elongation zone. Because cell shapes in the cell division zone are disc shaped to nearly isodiametric, CMFs were predominantly transverse to the root's long axis but generally not to the cell's. This suggests either that CMF orientation is not responsible for determining all aspects of cell expansion in this region or that cells establish transverse CMF patterns some time prior to the phase of highly anisotropic expansion. The finding that tightly transverse CMF alignment is established before CMTs are tightly transverse, together with data that indicate that CMTs become transverse only after elongation commences (Bichet et al., 2000; Wenzel et al., 2000), questions whether CMTs control CMF alignment at this stage of development. Similar doubts were raised in a recent study that showed CMT randomization when cellulose synthesis was inhibited (Fisher and Cyr, 1998).

In the distal elongation zone, CMTs were oblique to longitudinal, while CMFs remained transverse. Lack of CMT/CMF parallelism in post elongation zones has previously been reported (Hogetsu, 1986; Traas and Derksen, 1989; Baskin et al., 1999). A time lag before cellulose synthase complexes change their direction in response to changes in CMT orientation could explain the disconnection, but by plotting the x axis of Figure 7 as time instead of distance, we calculate this lag time at 4.5 h, which is more than half of the estimated 8-h cell elongation period. Alternatively, CMT-dependent alignment mechanisms could cease well before growth arrest, but CMFs might continue to use already deposited cell wall layers as templates. It is also conceivable that cellulose synthesis might be reduced as cell expansion slows so that the observed CMFs in older cells might have been laid down prior to changes in CMT orientation. Examining the spatial distribution of cellulose synthesis along the long axis of roots will help test this third possibility.

CONCLUSION

Our results indicate that close CMT/CMF coalignment occurs only in the proximal elongation

zone when REGRs are increasing. Throughout development, CMF orientation is more consistently transverse than CMT orientation, a result that questions the nature of the relationship between CMT and CMF alignment. We are currently applying these methods to examine CMT and wall patterns in Arabidopsis roots challenged by drugs or mutations that target cell wall or CMT-specific functions. By using this approach we hope to improve the understanding of wall construction in plant cells.

MATERIALS AND METHODS

Plant Material and Growth Conditions

Arabidopsis ecotype Columbia was used throughout this study. Seeds were surface sterilized in a mixture of 3% (v/v) hydrogen peroxide and 50% (v/v) ethanol for 2 min. After rinsing in sterilized water, seeds were planted on nutrient-solidified agar (Bacto Agar, DIFCO Laboratories, Detroit) plates [2 mM KNO_3, 5 mM $Ca(NO_3)_2$, 2 mM $MgSO_4$, 1 mM KH_2PO_4, 90 μM iron-EDTA complex, 46 μM H_3BO_3, 9.2 μM $MnCl_2$, 0.77 μM $ZnSO_4$, 0.32 μM $CuSO_4$, 0.11 μM MoO_3, 1% (w/v) Glc, 1.2% (w/v) agar, 530 μM myo-inositol, and 50 μM thiamine hydrochloride]. Plates were sealed with laboratory film and held vertically in a growth cabinet under constant light (80 μmol m^{-2} s^{-1}) and temperature (21°C).

Measurement of Root Growth

To measure the rate of root elongation, the position of the root apex was scored with a razor blade on the outside of plastic Petri plates every 12 h. At the end of experiments each plate was photocopied and the distance between each mark was measured using the digital image analysis program, Image I (Universal Imaging, West Chester, PA). Root diameter was measured approximately 0.5 mm from the root apex using a dissection microscope (SMZ-2T, Nikon, Tokyo) equipped with an ocular micrometer. Average elongation rates and root diameters with SD were calculated from data on at least 30 roots grown in three different plates.

Growth Kinetics

To examine the spatial distribution of elongation along roots, carbon grains were applied to the upper surface of roots with an eyelash and their positions photographed at 1-h intervals (Fig. 1). Separation of carbon grains at specific distances from root tips was measured on photographic prints using Image I software and REGRs were calculated as follows:

$$\text{REGR } (h^{-1}) = \frac{\ln x_f - \ln x_i}{t}$$

where x_f is the final distance between two carbon grains, x_i is the initial distance between two carbon grains, and t is the time interval.

Cell Wall Preparation

Whole seedlings were fixed in 4% (v/v) formaldehyde made up PEM buffer (25 mM PIPES [1,4-piperazinediethanesulfonic acid], 0.5 mM $MgSO_4$, 2.5 mM EGTA, pH 7.2), rinsed three times in PEM buffer, and cryoprotected in 25% and 50% (v/v) DMSO (in PME buffer, 10 min each step). Root tips were excised with a razor blade, placed on a nail head, and immediately frozen in liquid nitrogen. After slicing off the surface of a root with a glass knife on a cryo-ultra-microtome (Ultracut E ultra-microtome with FC 4 cryo-microtomy attachment, Reichert-Jung, Vienna), while maintaining samples and knives at −120°C, the remaining portion of the root was thawed in 50% (v/v) DMSO, and then transferred into PEM buffer. Several different treatments were tested to extract membranes and other cytoplasmic materials: (a) chloroform/methanol (1:1) twice for 1 h at 40°C, followed by methanol and acetone treatment, each for 30 min; (b) 1% (v/v) saponin for 48 h at 30°C; (c) 1% (v/v) Triton X-100 for 48 h at 30°C; (d) 0.1% (v/v) sodium hypochlorite for 10 min; (e) boiling in acetic acid and nitric acid and distilled water (8:1:2) for 1 h. After thoroughly rinsing in distilled water, osmication in cold 0.5% (v/v) OsO_4 for 15 min, rinsing in distilled water, and dehydration through a graded ethanol series (30%, 50%, 70%, 95%, and 100% three times, 15 min for each step), specimens were critical point dried using CO_2.

FESEM

All specimens were mounted on stubs with double-sided sticky carbon tape, cut surface facing upward, and coated with platinum at 2.4 mA for 195 s. Cell wall fine structure was examined on a Hitachi S4500 FESEM (Hitachi, Tokyo), fitted with a solid state backscattered upper electron detector at 5 kV. The condenser lens was set between 8 and 9 with a working distance between 5 and 8. Scanned images were recorded with Image slave 2.11 (Meeco, Melbourne).

Cell Wall Digestion by Enzymes

To identify the chemical basis of cell wall structures observed by FESEM, root specimens were treated with several polysaccharide-degrading enzymes and proteases before treatment with 0.1% (v/v) sodium hypochlorite. Tested enzymes were (a) 0.1% (w/v) Cellulysin (Calbiochem-Novabiochem, San Diego) in PEM buffer for 1 h at root temperature, (b) 0.1% (w/v) Pectolyase Y-23 (Kikkoman, Tokyo) in PME buffer for 30 min at room temperature, (c) 0.125 units mL^{-1} endo-1,4-β-glucanase (Megazyme International, Bray, County Wicklow, Ireland) in 50 mM sodium acetate (pH 4.7) for 5 h at 37°C, (d) 0.1% (w/v) Pronase (Boehringer Mannheim, Mannheim, Germany) in Tris-buffered saline (pH 7.4) for 1 h at room temperature.

Immunofluorescence

Whole seedlings were fixed in 1.5% (v/v) formaldehyde and 0.5% (v/v) glutaraldehyde made up in PEMT buffer

(50 mM PIPES, 2 mM EGTA, 2 mM $MgSO_4$, 0.05% [v/v] Triton X-100, pH 7.2) for 40 min and rinsed in PEMT buffer three times for 10 min. They were subsequently digested with 0.05% (w/v) Pectolyase Y-23 (Kikkoman) in PEM buffer (50 mM PIPES, 2 mM EGTA, 2 mM $MgSO_4$) with 0.4 M mannitol for 20 min, rinsed in PEM buffer three times, treated with −20°C methanol for 10 min, and rehydrated in phosphate-buffered saline (PBS) for 10 min. Autofluorescence caused by free aldehydes from glutaraldehyde fixation was reduced with 1 mg mL^{-1} $NaBH_4$ in PBS for 20 min, followed by the treatment with 50 mM Gly in PBS (incubation buffer) for 30 min. Seedlings were incubated with primary antibodies against tubulin at room temperature overnight, rinsed in incubation buffer three times for 10 min, and secondary antibodies applied for 3 h at 37°C. After rinsing in PBS three times, root tips were cut off from the rest of seedlings, and mounted in 0.1% (w/v) paraphenylene diamine in 1:1 PBS-glycerol, pH 9. Cut cover glasses were used to space slide and cover glasses so as to avoid crushing delicate root tips.

Antibodies

For this study, anti-β tubulin (product N357, Amersham, Buckinghamshire, England) was used at a dilution of 1:100. Fluorescein isothiocyanate-conjugated anti-mouse IgG (Silenus/Amrad Biotech, Boronia, Victoria, Australia), diluted 1:100, was used as a secondary antibody.

Confocal Laser Scanning Microscopy

Immunofluorescence images were collected with an MRC- Bio-Rad 600 (Microscience Division, Hemel Hempstead, UK) confocal laser-scanning microscope, coupled to a Zeiss Axiovert IM-10 inverted microscope. Excitation at 488 nm with an argon ion laser was used for fluorescein isothiocyanate fluorochromes. Images were collected using a Plan Neofluar 100-X objective lens, N.A. 1.30, following Kalman averaging of six full scans. Three-dimensional images from the root apex to the differentiation zone were obtained by collecting series of approximately 60 optical sections, each section approximately 0.6 μm thick, in the *Z* axis. Images were processed with image processing software programs including COMOS 7.0 (Microscience Division, Hemel Hempstead, UK), Confocal assistant 4.02 (written by Todd Clark Brelje) and Adobe Photoshop 4.0 (Adobe Systems, Mountain View, CA). All confocal images were flipped about the vertical axis to adjust for the inverted stage of our microscope.

Measurement and Analysis of Microtubule and Cellulose Alignment

The alignments of CMTs and CMFs were measured from printed images obtained by confocal microscopy and FESEM, respectively. Angular deviation from the longitudinal axis of roots was measured with Image I software. Transverse orientation was defined as 90° to the long axis plotted along the right vertical axis of the image, as viewed from the outside of the cell (as happened in immunofluorescence) so that FESEM images (taken looking from inside the cell) were flipped. Elements aligned at angles between 0° and 90° (counterclockwise from top) formed a left-handed helix while those elements oriented between 90° and 180° formed a right-handed helix. For CMTs, each data point represented a total of 60 CMTs from six different roots. CMF measurements were taken from 2.4 μm × 1.5 μm wall patches, which were sampled from several adjacent cells at each distance from the apex. Regions around pit fields were avoided. Each data point represented a total of 300 CMFs, combined from 30 wall patches from three different roots. SD was calculated from CMT and CMF angular measurements. Means between data points were compared by the independent Student's *t* test for samples with unequal variance (Microsoft EXCEL), at a significance level of 0.001. In general, microfibrils were straight and uniformly aligned across the observed window, except occasionally they appeared slightly wavy. Very little variation between sample windows or between cells at a similar position was observed. Fixation and all other processes involved for the FESEM preparation did not cause any major artifact so that the great majority of cells could be analyzed.

ACKNOWLEDGMENTS

We thank Frank Brink, Sally Stowe, and David Vowles of the ANU Electron Microscopy Unit for their assistance and tuition with the FESEM technique, and Tobias Baskin, Brian Gunning Nori Hasenbein, and Owen Schwartz for helpful advice.

Received August 9, 2000; modified September 14, 2000; accepted September 27, 2000.

LITERATURE CITED

Abe H, Funada R, Imaizumi H, Ohtani J, Fukazawa K (1995) Dynamic changes in the arrangement of cortical microtubules in conifer tracheids during differentiation. Planta **197:** 418–421

Arioli T, Peng L, Betzner AS, Burn J, Wittke W, Herth W, Camilleri C, Hofte H, Plazinski J, Birch R, Cork A, Glover J, Redmond J, Williamson RE (1998) Molecular analysis of cellulose biosynthesis in *Arabidopsis*. Science **279:** 717–720

Baluska F, Parker JS, Barlow PW (1992) Specific pattern of cortical and endoplasmic microtubules associated with cell growth and tissue differentiation in roots of maize (*Zea mays* L). J Cell Sci **103:** 191–200

Baskin TI, Betzner AS, Hoggart R, Cork A, Williamson RE (1992a) Root morphology mutants in *Arabidopsis thaliana.* Aust J Plant Physiol **19:** 427–438

Baskin TI, Busby CH, Fowke LC, Sammut M, Gubler F (1992b) Improvements in immunostaining samples embedded in methacrylate: localization of microtubules and other antigens throughout developing organs in plants of diverse taxa. Planta **187:** 405–413

Baskin TI, Cork A, Williamson RE, Gorst JR (1995) *STUNTED PLANT 1*, a gene required for expansion in rapidly elongating but not dividing cells and mediating root growth responses to applied cytokinin. Plant Physiol **107:** 233–243

Baskin TI, Meekes HTHM, Liang BM, Sharp RE (1999) Regulation of growth anisotropy in well-watered and water-stressed maize roots: II. Role of cortical microtubules and cellulose microfibrils. Plant Physiol **119:** 681–692

Benfey PN, Schiefelbein JW (1994) Insights into root development from *Arabidopsis* root mutants. Plant Cell Environ **17:** 675–680

Bichet A, Desnos T, Turner S, Grandjean O, Höfte H (2000) *BOTERO1* is required for normal orientation of cortical microtubules and anisotropic cell expansion in *Arabidopsis*. Plant J (in press)

Brown RM Jr (1982) Cellulose and Other Natural Polymer Systems: Biogenesis, Structure and Degradation. Plenum Press, New York

Carpita NC, Gibeaut DM (1993) Structural models of primary cell walls in flowering plants: consistency of molecular structure with the physical properties of the walls during growth. Plant J **3:** 1–30

Clayton L, Black CM, Lloyd CW (1985) Microtubule nucleating sites in higher plant cells identified by an autoantibody against pericentriolar material. J Cell Biol **101:** 319–324

Collings DA, Winter H, Wyatt SE, Allen NS (1998) Growth dynamics and cytoskeleton organization during stem maturation and gravity-induced stem bending in *Zea mays* L. Planta **207:** 246–258

Cosgrove DJ (1997) Relaxation in a high-stress environment: the molecular bases of extensible cell walls and cell enlargement. Plant Cell **9:** 1031–1041

Crewe AV, Eggenberger DN, Wall J, Welter LM (1968) Electron gun using a field emission source. Rev Sci Inst **39:** 576–584

Dolan L, Janmaat K, Willemsen V, Linstead P, Poethig S, Roberts K, Scheres B (1993) Cellular organisation of the *Arabidopsis thaliana* root. Development **119:** 71–84

Emons AMC (1988) Methods for visualizing cell wall architecture. Acta Bot Neerl **37:** 31–38

Esau K (1977) Anatomy of Seed Plants. John Wiley & Sons, New York

Falconer MM, Seagull RW (1986) Xylogenesis in tissue culture: II. Microtubule, cell shape and secondary wall patterns. Protoplasma **133:** 140–148

Fisher DD, Cyr RJ (1998) Extending the microtubule/microfibril paradigm: cellulose synthesis is required for normal cortical microtubule alignment in elongating cells. Plant Physiol **116:** 1043–1051

Flanders DJ, Rawlins DJ, Shaw PJ, Lloyd CW (1990) Re-establishment of the interphase microtubule array in vacuolated plant cells, studied by confocal microscopy and 3-D imaging. Development **110:** 897–904

Galway ME, Hardham AR (1986) Microtubule reorganization, cell wall synthesis and establishment of the axis of elongation in regenerating protoplasts of the alga *Mougeotia*. Protoplasma **135:** 130–143

Galway ME, Hardham AR (1989) Oryzalin induced microtubule disassembly and recovery in regenerating protoplasts of the alga *Mougeotia*. J Plant Physiol **135:** 337–345

Giddings TH, Staehelin LA (1991) Microtubule-mediated control of microfibril deposition: a re-examination of the hypothesis. *In* CW Lloyd, ed, The Cytoskeletal Basis of Plant Growth and Form. Academic Press, New York, pp 85–100

Green PB (1958) Structural characteristics of developing Nitella internodal cell walls. J Biophys Biochem Cytol **4:** 505–516

Green PB (1962) Mechanism of plant cell morphogenesis. Science **138:** 1404–1405

Gunning BES, Hardham AR (1982) Microtubules. Annu Rev Plant Physiol **33:** 651–698

Hardham AR, Green PB, Lang JM (1980) Reorganization of cortical microtubules and cellulose deposition during leaf formation in *Graptopetalum paraguayense*. Planta **149:** 181–195

Hasezawa S, Nozaki H (1999) Role of cortical microtubules in the orientation of cellulose microfibril deposition in higher-plant cells. Protoplasma **209:** 98–104

Hauser M-T, Morikami A, Benfey PN (1995) Conditional root expansion mutants of *Arabidopsis*. Development **121:** 1237–1252

Herth W (1980) Calcofluor white and congo red inhibit chitin microfibril assembly of *Poterioochromonas*: evidence for a gap between polymerization and microfibril formation. J Cell Biol **87:** 442–450

Hogetsu T (1986) Orientation of wall microfibril deposition in root cells of *Pisum sativum* L. var Alaska. Plant Cell Physiol **27:** 947–951

Hogetsu T, Oshima Y (1986) Immunofluorescence microscopy of microtubule arrangement in root cells of *Pisum sativum* L. var. Alaska. Plant Cell Physiol **27:** 939–945

Hogetsu T, Shibaoka H (1978) Effects of colchicine on cell shape and on microfibril arrangement in the cell wall of *Closterium acerosum*. Planta **140:** 15–18

Itoh T (1976) Microfibrillar orientation of radially enlarged cells of coumarin- and colchicine-treated pine seedlings. Plant Cell Physiol **17:** 385–398

Kimura S, Mizuta S (1994) Role of the microtubule cytoskeleton in alternating changes in cellulose microfibril orientation in the coenocytic green alga, *Chaetomorpha moniligera*. Planta **193:** 21–31

Knox JP (1992) Molecular probes for the plant surface. Protoplasma **167:** 1–9

Kropf DL, Williamson RE, Wasteneys GO (1997) Microtubule orientation and dynamics in elongating characean internodal cells following cytosolic acidification, induction of pH bands, or premature growth arrest. Protoplasma **197:** 188–198

Lang JM, Eisinger WR, Green PB (1982) Effects of ethylene on the orientation of microtubules and cellulose microfibrils of pea epicotyl cells with polylamellate cell walls. Protoplasma **110:** 5–14

Laskowski MJ (1990) Microtubule orientation in pea stem cells: a change in orientation follows the initiation of growth rate decline. Planta **181:** 44–52

Liang BM, Dennings AM, Sharp RE, Baskin TI (1996) Consistent handedness of microtubule helical arrays in maize and *Arabidopsis* primary roots. Protoplasma **190:** 8–15

Marc J, Hackett WP (1989) A new method for immunofluorescent localization of microtubules in surface cell layers: application to the shoot apical meristem of *Hedera*. Protoplasma **148:** 70–79

Marchant HJ, Hines ER (1979) The role of microtubules and cell-wall deposition in elongation of regenerating protoplasts of *Mougeotia*. Planta **146:** 41–48

McCann MC, Roberts K (1991) Architecture of the primary cell wall. *In* CW Lloyd, ed, The Cytoskeletal Basis of Plant Growth and Form. Academic Press, New York, pp 109–129

McCann MC, Wells B, Roberts K (1990) Direct visualization of cross-links in the primary plant cell wall. J Cell Sci **96:** 323–334

McClinton RS, Sung ZR (1997) Organization of cortical microtubules at the plasma membrane in *Arabidopsis.* Planta **201:** 252–260

Mueller SC, Brown RM Jr (1980) Evidence for an intramembrane component associated with a cellulose microfibril-synthesizing complex in higher plants. J Cell Biol **84:** 315–326

Mullen JL, Ishikawa H, Evans ML (1998) Analysis of changes in relative elemental growth rate in the elongation zone of *Arabidopsis* roots upon gravistimulation. Planta **206:** 598–603

Nagata T, Hasezawa S (1993) Events at the border between the M and G_1 phases in highly synchronized culture of tobacco BY-2 cells. J Plant Res Suppl **3:** 29–35

Palevitz BA, Hepler PK (1976) Cellulose microfibril orientation and cell shaping in developing guard cells of *Allium*: the role of microtubules and ion accumulation. Planta **132:** 71–93

Pawley JB, Erlandsen SL (1989) The case for low voltage high resolution scanning electron microscopy of biological samples. Scanning Microsc Suppl **3:** 163–178

Preston RD (1974) The Physical Biology of Plant Cell Walls. Chapman and Hall, London, p 491

Preston RD (1988) Cellulose-microfibril-orienting mechanisms in plant cell walls. Planta **174:** 67–74

Pritchard J, Hetherington PR, Fry SC, Tomos AD (1993) Xyloglucan endotransglycosylase activity, microfibril orientation and the profiles of cell wall properties along growing regions of maize roots. J Exp Bot **44:** 1281–1289

Prodhan AKMA, Funada R, Ohtani J, Abe H, Fukuzawa K (1995) Orientation of microfibrils and microtubules in developing tension-wood fibers of Japanese ash (*Fraxinus mandshurica* var. *japonica*). Planta **196:** 577–585

Richmond PA (1983) Patterns of cellulose microfibril deposition and rearrangement in *Nitella*: *in vivo* analysis by a birefringence index. J Appl Poly Sci **37:** 107–122

Roberts IN, Lloyd CW, Roberts K (1985) Ethylene-induced microtubule reorientation: mediation by helical arrays. Planta **164:** 439–447

Robinson DG, Quader H (1982) The microtubule-microfibril syndrome. *In* CW Lloyd, ed, The Cytoskeleton in Plant Growth and Development. Academic Press, New York, pp 109–126

Sassen MMA, Traas JA, Wolters-Arts AMC (1985) Deposition of cellulose microfibrils in cell walls of root hairs. Eur J Cell Biol **37:** 21–26

Sauter M, Seagull RW, Kende H (1993) Internodal elongation and orientation of cellulose microfibrils and microtubules in deepwater rice. Planta **190:** 354–362

Sawhney VK, Srivastava LM (1975) Wall fibrils and microtubules in normal and gibberellic-acid-induced growth of lettuce hypocotyl cells. Can J Bot **53:** 824–835

Seagull RW (1986) Changes in microtubule organization and microfibril orientation during in vitro cotton fiber development: an immunofluorescent study. Can J Bot **64:** 1373–1381

Seagull RW, Heath IB (1980) The organization of cortical microtubule arrays in the radish root hair. Protoplasma **103:** 205–229

Srivastava LM, Sawhney VK, Bonnettemaker M (1976) Cell growth, wall deposition, and correlated fine structure of colchicine-treated lettuce hypocotyl cells. Can J Bot **55:** 902–917

Taiz L (1984) Plant cell wall expansion: regulation of cell wall mechanic properties. Annu Rev Plant Physiol **35:** 585–653

Takeda K, Shibaoka K (1978) The fine structure of the epidermal cell wall in azuki bean epicotyl. Bot Mag **91:** 235–245

Takesue K, Shibaoka H (1999) Auxin-induced longitudinal-to-transverse reorientation of cortical microtubules in non-growing epidermal cells of azuki bean epicotyls. Protoplasma **206:** 27–30

Traas JA, Braat P, Derksen JW (1984) Changes in microtubule arrays during the differentiation of cortical root cells of *Raphanus sativus.* Eur J Cell Biol **34:** 229–238

Traas JA, Derksen J (1989) Microtubules and cellulose microfibrils in plant cells: simultaneous demonstration in dry cleave preparations. Eur J Cell Biol **48:** 159–164

Vesk PA, Rayns DG, Vesk M (1994) Imaging of plant microtubules with high resolution scanning electron microscopy. Protoplasma **182:** 71–74

Vesk PA, Vesk M, Gunning BES (1996) Field emission scanning electron microscopy of microtubule arrays in plant cells. Protoplasma **195:** 168–181

Wasteneys GO, Williamson RE (1987) Microtubule orientation in developing internodal cells of *Nitella*: a quantitative analysis. Eur J Cell Biol **43:** 14–22

Wasteneys GO, Williamson RE (1993) Cortical microtubule organization and internodal cell maturation in *Chara corallina*. Bot Acta **106:** 136–142

Wenzel CL, Williamson RE, Wasteneys GO (2000) Gibberellin-induced changes in growth anisotropy precede gibberellin-dependent changes in cortical microtubule orientation in developing epidermal cells of barley leaves: kinematic and cytological studies on a gibberellin-responsive dwarf mutant, M489. Plant Physiol **124:** 813–822

Wick SM (1985) Immunofluorescence microscopy of tubulin and microtubule arrays in plant cells: III. Transition between mitotic/cytokinetic and interphase microtubule arrays. Cell Biol Int Rep **9:** 357–371

Willats WGT, Knox JP (1999) Immunoprofiling of pectic polysaccharides. Anal Biochem **268:** 143–146